Supervisor Control for a Stand-Alone Hybrid Generation System Using Wind and Photovoltaic Energy

Fernando Valenciaga and Paul F. Puleston

***Abstract*—A comprehensive supervisor control for a hybrid system that comprises wind and photovoltaic generation subsystems, a battery bank, and an ac load is developed in this paper. The objectives of the supervisor control are, primarily, to satisfy the load power demand and, second, to maintain the state of charge of the battery bank to prevent blackout and to extend the life of the batteries. For these purposes, the supervisor controller determines online the operation mode of both generation subsystems, switching from power regulation to maximum power conversion. Decision criteria for the supervisor based on measurable system variables are presented. Finally, the performance of the supervisor controller is extensively assessed through computer simulation using a comprehensive nonlinear model of the plant.**

***Index Terms*—Power control, solar energy, wind energy.**

I. Introduction

THE rising rate of consumption of nuclear and fossil fuels has drawn worldwide attention to alternative energy technologies. In developed areas, such as the U.S. or the European Union, wind power has been the fastest-growing energy for the last decade, thanks to its increasingly attractive economics, its substantial environmental advantages, and supportive energy policies. However, it is in developing countries where the wind power (in combination with other renewable energies) can play a more substantial role to dramatically improve the quality of life of the people in the immediate future. Particularly, in Latin America, many people live in isolated areas far from the main utility grid. The inability of electrical utilities to meet their needs is a special concern to small rural-based households, schools, and enterprises [1]. It has been proven that small-to-medium-size (10–100 kW) hybrid generation systems based on wind and solar sources may electrify villages, powering lamps and small appliances, small industries, health clinics, and school and community centers [2].

In this international expanding context, research in the field of new technologies for wind energy conversion systems (WECS) and hybrid systems has become a crucial effort. It has been established that together with improvements in materials, power electronics, and blade design, the incorporation of advanced control systems into the WECS is one of the major technology changes that has translated into reduced costs of energy [3], turning the development of high-efficiency control strategies for WECS into an essential R&D activity.

Presently, such a control challenge can be tackled thanks to the cost reduction and improvement of power semiconductors, ac drives, and microprocessors. Despite the extra initial investment, the inclusion of electrical control permits a higher degree of flexibility and more complex objectives can be achieved, particularly in variable-speed operation control [4]–[7]. With these technological improvements at hand, classic controllers for WECS can be updated by the development of more efficient strategies based on modern control techniques such as: fuzzy logic control [8], robust control [9], adaptive control [10], etc. Among them, sliding-mode (SM) control emerges as an especially suitable option to deal with variable-speed operating WECS electronically controlled. This control technique has proven to be very robust with respect to system parameter variations and external disturbances [11], [12]. Its use for the design of novel control strategies for various applications of grid-connected WECS and autonomous electric generation hybrid systems (EGHS) has been presented in several papers by the authors [13]–[15]. Other recent example of SM utilized for WECS control applications can be found in [16] and [17].

From the reasons exposed above, it can be clearly inferred that the development of novel control strategies for grid-connected and stand-alone WECS is not merely an area of research plenty of challenging problems from the control design point of view, but also and principally a field of technological R&D activity of high interest for environmental, social, economical, and strategic reasons.

II. Fundaments on Hybrid Systems

Stand-alone hybrid generation systems are usually used to supply isolated areas or locations interconnected to a weak grid. They combine several generation modules, typically assimilating different renewable energy sources. The application of these hybrid topologies reduces the probability of energy supply shortage and, with the incorporation of energy storage, it allows to eliminate the background diesel generator (which is commonly required in generation systems based on a single renewable energy source). In this context, many EGHS frequently combine solar and wind energy sources (taking advantage of their complementary nature) with a lead-acid battery bank (to overcome periods of scarce generation).

Manuscript received April 29, 2003; revised April 2, 2004. This work was supported by CONICET, SECyT, and La Plata National University (UNLP), La Plata, Argentina. Paper no. TEC-00106-2003.

The authors are with CONICET and the LEICI, Faculty of Engineering, La Plata National University, La Plata 1900, Argentina (e-mail: fval@ing.unlp.edu.ar; puleston@ing.unlp.edu.ar).

Digital Object Identifier 10.1109/TEC.2005.845524

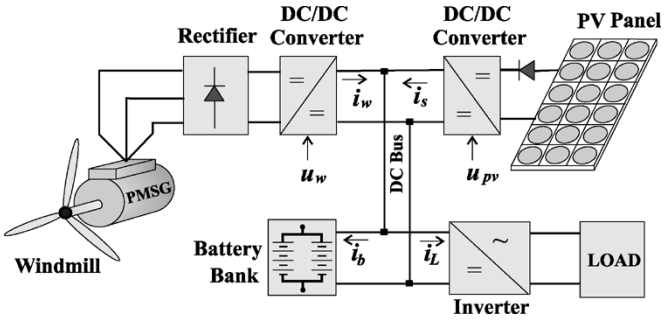

Fig. 1. Hybrid generation system.

The topology of the hybrid system under consideration in this paper is depicted in Fig. 1. The wind generation module is constituted by a windmill, a multipolar permanent-magnet synchronous generator (PMSG), a rectifier, and a dc/dc converter to interface the generator with the dc bus. The converter commands the voltage on the PMSG terminals, indirectly controlling the operation point of the wind turbine and, consequently, its power generation.

The solar module comprises several PV panels connected to the dc bus via a dc/dc converter. Similar to the wind subsystem, the converter controls the operation point of the PV panels. The dc bus collects the energy generated by both modules and delivers it to the load and, if necessary, to the battery bank. Its voltage is imposed by the battery bank which comprises lead-acid batteries connected in a serial/parallel array. The load could be an ac or a dc load. In the case under analysis, it is assumed to be an ac load; therefore, a voltage inverter is required.

The cost of the battery bank plays a fundamental role in the overall system cost [18]. This is a critical reason to operate the battery bank carefully, with the objective of extending its operative life. Many lead-acid battery manufacturers recommend specific recharge cycles to recover 100% of the charge capacity and also to protect the battery against dehydration. The recommended recharge cycle comprises a *recovery period* and a *maintenance period*, both carried out with different constant current values. Therefore, it is required that the current reference of the battery bank $(I_{b\,\mathrm{ref}})$ follows the specified recharge cycle.

III. System Models

A. Wind Subsystem

The model of the wind subsystem written in a rotor reference frame can be expressed by [13]

$$\dot{x} = \begin{bmatrix} \dot{i}_q \\ \dot{i}_d \\ \dot{\omega}_e \end{bmatrix} = \begin{bmatrix} f_1 \\ f_2 \\ f_3 \end{bmatrix} + \begin{bmatrix} g_1 \\ g_2 \\ g_3 \end{bmatrix} u_w$$

$$= \begin{bmatrix} -\frac{r_s}{L} i_q - \omega_e i_d + \frac{\omega_e \phi_{sr}}{L} \\ -\frac{r_s}{L} i_d + \omega_e i_q \\ \frac{P}{2J}\left(T_t - \frac{3}{2}\frac{P}{2}\phi_{sr} i_q\right) \end{bmatrix} + \begin{bmatrix} -\frac{\pi \mathrm{v}_b i_q}{3\sqrt{3}L\sqrt{i_q^2+i_d^2}} \\ -\frac{\pi \mathrm{v}_b i_d}{3\sqrt{3}L\sqrt{i_q^2+i_d^2}} \\ 0 \end{bmatrix} u_w$$

$$i_w = \frac{\pi}{2\sqrt{3}}\sqrt{i_q^2 + i_d^2}\, u_w \tag{1}$$

where i_d and i_q are, respectively, the direct current and the quadrature current in the rotor reference frame; ω_e is the electrical angular speed; r_s and L are the per phase resistance and inductance of the stator windings, respectively; P is the PMSG number of poles; J is the inertia of the rotating parts; ϕ_{sr} is the flux linked by the stator windings; v_b is the voltage on the battery bank terminals; u_w is the control signal (duty cycle of the dc/dc converter), i_w is the current injected on the dc bus; and T_t is the wind turbine torque. The latter may be written as

$$T_t = \frac{1}{2} C_t(\lambda) \rho A R v^2 \tag{2}$$

where ρ is the air density, A is the turbine swept area, R is the turbine radio, v is the wind speed, and $C_t(\lambda)$ is a nonlinear torque coefficient which depends on the tip speed ratio ($\lambda = R\omega_m/v$, with $\omega_m = \omega_e 2/P$ the angular shaft speed).

Equations (1) and (2) show the highly nonlinear dynamic behavior of the power generation wind module. From (1), the power injected by the wind subsystem into the dc bus can be written as

$$P_w = \frac{\pi \mathrm{v}_b}{2\sqrt{3}}\sqrt{i_q^2 + i_d^2}\, u_w. \tag{3}$$

This equation shows the wind-generated power dependence on the control signal u_w, which controls the power injected by this module into the dc bus.

B. Solar Subsystem

The solar power generating subsystem consists of a PV panel array and a half-bridge buck dc/dc converter. The dynamic model of this subsystem can be expressed as [14]

$$\dot{\mathrm{v}}_{\mathrm{pv}} = \frac{i_{\mathrm{pv}}}{C} - \frac{i_s}{C} u_{\mathrm{pv}} \tag{4}$$

$$\dot{i}_s = -\frac{\mathrm{v}_b}{L} + \frac{\mathrm{v}_{\mathrm{pv}}}{L} u_{\mathrm{pv}} \tag{5}$$

$$i_{\mathrm{pv}} = n_p I_{ph} - n_p I_{rs}\left(e^{\frac{q(\mathrm{v}_{\mathrm{pv}} + i_{\mathrm{pv}} R_s)}{n_s A_c K T}} - 1\right) \tag{6}$$

where v_{pv} is the voltage level on the PV panel array terminals, i_s is the current injected on the dc bus, C and L are electrical parameters of the buck converter, u_{pv} is the control signal (duty cycle), and i_{pv} is the current generated by the PV array. In (6), n_s is the number of PV cells connected in series; n_p is the number of series strings in parallel; K is the Boltzman constant; A_c is the cell deviation from the ideal p-n junction characteristic; I_{ph} is the photocurrent; and I_{rs} the reverse saturation current. The power injected by the PV solar module into the dc bus could be written as

$$P_s = i_s \mathrm{v}_b. \tag{7}$$

It should be noted that this power indirectly depends on the control signal u_{pv}.

IV. Operation Strategy and Supervisor Control

A. General Description of the Supervisor Control Policy

The capability of the EGHS to satisfy the power demand depends on the atmospheric conditions. Such conditions and the role of the battery bank (either storing or supplying energy) will

define different operation modes of the system. Basically, these operation modes are determined by the energy balance between the total generation (wind and solar) and the total demand (load demand plus the required power to recharge the battery bank). A comprehensive supervisor control algorithm is essential to efficiently manage the operation of the generation subsystems according to those modes.

For the design of such supervisor control, in the first place, it has been decided that the main generation role would be in charge of the wind subsystem while the solar subsystem would play a complementary role. Note that the original motivation for this design decision was that it was taken from the viewpoint of applications in geographical areas with wealthy wind regimes (particularly, bearing in mind Patagonia). However, this is not at all a limitation of the control proposal, provided that the results presented below can straightforwardly be extended considering the solar subsystem as the main supplier and the wind subsystem playing the secondary role.

The three possible modes of generation are as follows.

Mode 1) It corresponds to periods of sufficient wind power to satisfy the total demand. Therefore, the wind subsystem has to track the total demand while the solar subsystem is inactive and the battery bank is storing energy following the recharge cycle. This situation is maintained until the total power demand exceeds the maximum available wind power. Beyond that limit, the supervisor control switches to *Mode 2*, activating the solar module.

Mode 2) The supervisor control sets the wind subsystem for maximum generation (i.e., operation at the point of maximum energy conversion) and the solar subsystem is set to track a power reference. This reference corresponds to the power required to complement the wind generation and together satisfies the total power demand. It should be remarked that in *Modes 1* and *2*, the battery bank is not requested to supply power to the load. On the contrary, under these modes of operation, the battery bank demands the maintenance current or the recharge current and, consequently, becomes part of the total demand. Once the limit of maximum generation of the hybrid system is reached or exceeded by the total power demand, the system enters *Mode 3* of operation.

Mode 3) This mode of operation is characterized by both generation subsystems set to operate at their maximum energy conversion points. In addition, to fully satisfy the load demand, the battery bank is able to revert its energy flow, acting as power supplier instead as a recipient of energy. Note that operation in *Mode 3* can be maintained as long as the energy available in the battery bank is sufficient to complement the generation to satisfy the load requirements. If this limit is surpassed, the load must be disconnected to recharge batteries and avoid damages. Nevertheless, this situation is highly unlikely provided that the system modules were sized to reduce such a blackout situation to a minimum.

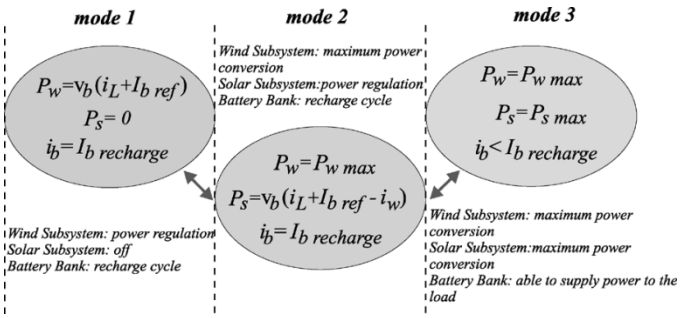

Fig. 2. Schematic description of the operation modes.

To summarize, the supervisor control is responsible for switching from one operation mode to another depending on the atmospheric conditions, the load demand, and the battery charge. Moreover, it is in charge of setting the reference values of the generation modules and the battery current for each mode of operation.

A schematic description of the operation strategy is depicted in Fig. 2.

B. Wind Subsystem Operation

As was previously established, the wind subsystem acts under the supervisor control directives either supplying the total load or tracking the operation point of maximum power conversion (*Mode 1* or *Mode 2/Mode 3*, respectively). In *Mode 1*, the control objective of the wind module is power regulation according to the following reference:

$$P_{w\ \mathrm{ref1}} = P_{\mathrm{Total\ demand}} = \mathrm{v}_b(i_L + I_{b\ \mathrm{ref}}) \tag{8}$$

where i_L is the load current [reflected to the dc bus side (Fig. 1)] and $I_{b\ \mathrm{ref}}$ is the desired current for the battery bank (according to the recharge cycle). The former is a measurable current while the latter is set by the supervisor control depending on the state of charge of the battery bank.

In the second case (*Mode 2/Mode 3*), the expression of the reference for maximum power conversion is not so straightforwardly obtained. Actually, it would be quite simple if the wind speed was measured; however, adequate wind speed information for control purposes is not always available. An alternative to circumvent the dependence on wind measurements is to neglect the high-frequency wind variations caused by gusts and turbulences, and then tracking an average maximum conversion point, instead of the instantaneous one. In this way, the control objective is equivalent to track the maximum power conversion point of a filtered version of the wind, avoiding sudden changes of torque and, consequently, reducing mechanical stress in the shaft. The objective of maximum conversion tracking without wind measurement can be attained by creating a power reference which relies only on few turbine parameters and on a simple measurement of the angular shaft speed

$$\begin{aligned} P_{w\ \mathrm{ref2}} &= P_{w\ \mathrm{opt}} - P_{\mathrm{losses}} \\ &= K_{\mathrm{opt}}\omega_m^3 - \frac{3}{2}\left(i_q^2 + i_d^2\right) r_s \end{aligned} \tag{9}$$

$$\text{where} \quad K_{\mathrm{opt}} = \frac{C_t(\lambda_{\mathrm{opt}})\rho A R^3}{2\lambda_{\mathrm{opt}}^2} \tag{10}$$

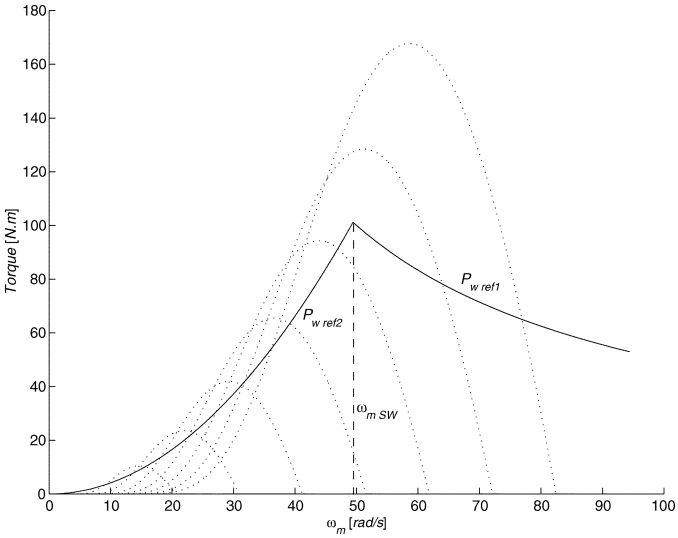

Fig. 3. Wind operation strategy in the plane torque—angular shaft speed.

being $\lambda_{\rm opt}$ the tip speed ratio that maximizes the power extracted to the wind.

In the torque-shaft speed plane (Fig. 3), the loci corresponding to both power references are plotted (solid lines) for a constant load current (i_L). In dotted lines depict the curves of the wind turbine torque with the wind speed as parameter. It can be observed that both reference curves have a point in common that demarks the boundary between the operational modes of the wind module (*Mode 1* on the right-hand side, and *Mode 2/Mode 3* on the left-hand side).

The angular shaft speed of the boundary point is given by

$$\omega_{m\ SW} = \sqrt[3]{\frac{P_{w\ \rm ref1} + \frac{3}{2}\left(i_q^2 + i_d^2\right) r_s}{K_{\rm opt}}} \tag{11}$$

then the supervisor control decides the mode of operation by comparing the measured speed with the boundary speed ω_{mSW}

$$\begin{cases} \text{if } \omega_m \geq \omega_{m\ SW}, \text{ then } Mode\ 1 \ \rightarrow \ P_{w\ \rm ref} = P_{w\ \rm ref1} \\ \text{if } \omega_m < \omega_{m\ SW}, \text{ then } Mode 2/3 \ \rightarrow \ P_{w\ \rm ref} = P_{w\ \rm ref2}. \end{cases} \tag{12}$$

Different control techniques can be proposed to fulfill those goals. In particular, in a previous work [19], the authors have developed an adaptive minimum-chattering SM controller especially intended for wind energy applications, presenting robust features and very good dynamic behavior for both control objectives under consideration in this section. Such control law can be incorporated into the framework of the supervisor control as follows, shown in the equation at the bottom of the page.

In (13), shown at the bottom, $s_{w1} = P_w - P_{w\ \rm ref1}$ and $s_{w2} = P_w - P_{w\ \rm ref2}$ are the sliding surfaces, γ and $\xi_{\max}$ are design parameters (namely, the reaching speed constant and the uncertainty bound, respectively) and x, $f_{\rm i}$ (with $\rm i = 1,2,3$) and $g_{\rm j}$ (with $\rm j = 1,2$) are system variables defined in (1).

C. Solar Subsystem Operation

The solar subsystem starts its operation when the wind power generation is insufficient to satisfy the total power demand. The supervisor control commands the solar subsystem either regulating power or tracking the PV maximum power conversion point (*Mode 2* or *Mode 3*, respectively). In *Mode 2*, the solar control objective is to complement the wind generation to satisfy the total power demand; therefore, the reference for the PV generated power results

$$P_{s\ \rm ref} = P_{\rm Total\ demand} - P_w = \mathrm{v}_b(i_L + I_{b\ \rm ref} - i_w). \tag{14}$$

In Fig. 4(a), the generated current of a PV panel array with fixed insolation and temperature (shown in the solid line) are presented along with the PV power reference $P_{s\ \rm ref}$ (dashed line) and the locus of maximum power conversion for different degrees of insolation (dashed-dotted line). In correspondence, Fig. 4(b) depicts the power–voltage plane, the PV generated power (solid line), the PV power reference (dashed line), and the locus of maximum power conversion (dashed-dotted line) for different atmospheric conditions. The intersection of the latter with the curve in solid line (point C) corresponds to the maximum power operation point (MPOP) of the PV array for those particular values of insolation and temperature.

In these figures, it can be appreciated that two operation points exist, capable of generating the reference power (points A and B). The characteristics of the buck dc/dc converter under consideration prevent the PV terminal voltage to reduce its value below v_b; therefore, the operation on the left-hand side of the MPOP (point A side) would be quite restrictive provided that the power regulation would be significantly bounded. Conversely, operating in the right-hand side of the MPOP (point B side) allows a broad range of power regulation; therefore, this side has been chosen for operation.

When the contribution of the PV array is not sufficient to satisfy the total power demand, the supervisor control switches to *Mode 3*. The solar subsystem objective becomes maximum power generation by continuously tracking the MPOP. A reliable criterion to decide when to switch from PV power regulation (*Mode 2*) to maximum power generation (*Mode 3*) must be deduced. Then, the first step is to establish the position of the MPOP (point C in Fig. 4) by zeroing the derivative of the power

$$\frac{\partial P_{\rm pv}}{\partial \mathrm{v}_{\rm pv}} = \frac{\partial\left(i_{\rm pv}(\mathrm{v}_{\rm pv}) \cdot \mathrm{v}_{\rm pv}\right)}{\partial \mathrm{v}_{\rm pv}} = \frac{\partial i_{\rm pv}}{\partial \mathrm{v}_{\rm pv}} \mathrm{v}_{\rm pv} + i_{\rm pv} = 0. \tag{15}$$

$$\begin{cases} \text{if } \omega_m \geq \omega_{m\ SW} \Rightarrow Mode\ 1: \\ \quad u_w = \left[-\frac{f_1}{g_1} + \frac{2K_{\rm opt}\omega_e f_3}{\phi_{sr} g_1} - \frac{i_q f_3}{g_1 \omega_e}\right] + 2\left(\gamma\left|s_{w2}(x)\right| + \xi_{m\acute{a}x}\left|\frac{\partial s_{w2}}{\partial x}\right|\right)\frac{\mathrm{sign}(s_{w2}(x))}{3\phi_{sr}\omega_e g_1} \\ \text{if } \omega_m < \omega_{m\ SW} \Rightarrow Mode\ 2/3: \\ \quad u_w = -\frac{\left[6r_s(i_q f_1 + i_d f_2) - 3\phi_{sr}(\omega_e f_1 + i_q f_3) + 2\left(\gamma|s_{w1}(x)| + \xi_{\max}\left|\frac{\partial s_{w1}}{\partial x}\right|\right)\mathrm{sign}(s_{w1}(x))\right]}{(6r_s(i_q g_1 + i_d g_2) - 3\phi_{sr}\omega_e g_1)} \end{cases} \tag{13}$$

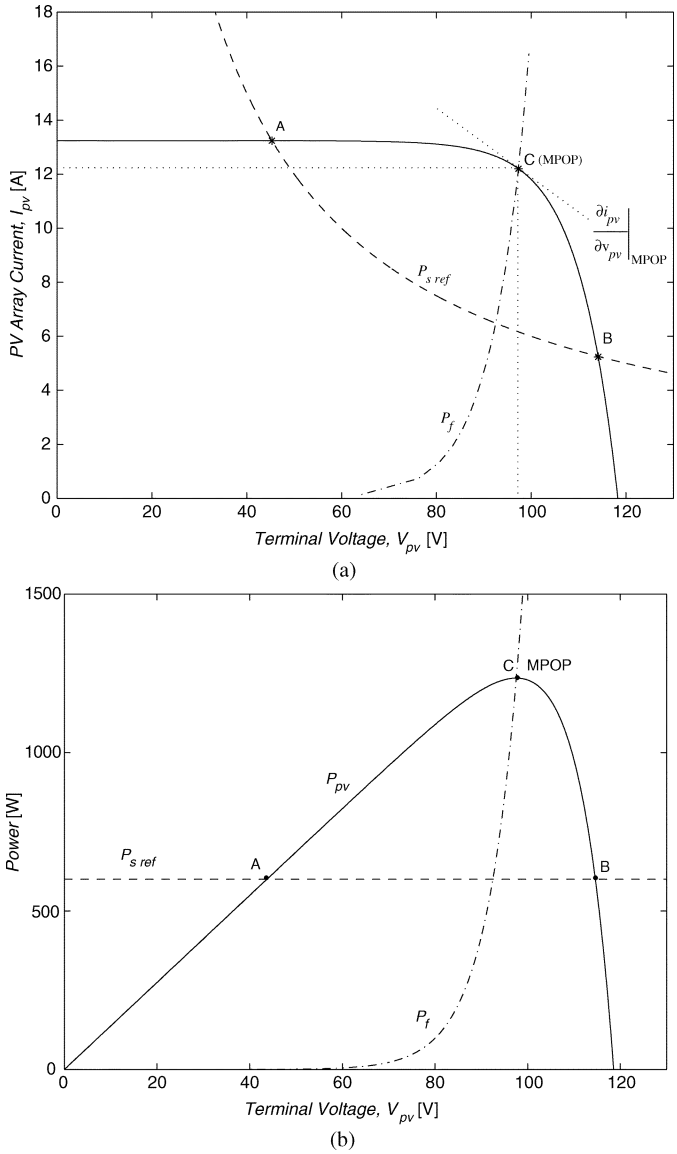

Fig. 4. (a) PV electrical characteristics and power reference. (b) PV power generation.

Next, from (15), the following expression can be defined:

$$-\frac{\partial i_{\rm pv}}{\partial {\rm v}_{\rm pv}}{\rm v}_{\rm pv}^2 \cong -\frac{\Delta i_{\rm pv}}{\Delta {\rm v}_{\rm pv}}{\rm v}_{\rm pv}^2 = P_f. \tag{16}$$

Evidently, (16) evaluated at the MPOP voltage provides the maximum solar power. However, when (16) is computed for other values of ${\rm v}_{\rm pv}$, it results not in actual power but in fictitious power P_f. Such fictitious power can be directly utilized to determine the mode of operation of the solar subsystem. Consider, for example, constant insolation and the subsystem regulating power (*Mode 2* operation) on a point situated on the right-hand side of the MPOP. It can be appreciated in Fig. 4(a) that in this side, the $i_{\rm pv}-{\rm v}_{\rm pv}$ curve presents a highly negative slope. Therefore, for any right-hand side operation, point P_f is greater than the power corresponding to the MPOP and, obviously, greater than the actual power at the present point of operation $(P_{s\,\rm ref})$. Then, if the operation point approached the MPOP, the actual PV power would also approach the fictitious power. The supervisor control can take advantage of this singularity to select the mode of operation according to

$$\begin{cases} \text{if } P_f \geq P_{s\,\rm ref}, & \text{then } Mode\,2: \text{ Power regulation} \\ \text{if } P_f < P_{s\,\rm ref}, & \text{then } Mode\,3: \text{ MPOP tracking.} \end{cases} \tag{17}$$

Similar to WECS applications, there exist several control alternatives to fulfill the objective of MPOP tracking. Some techniques reported in the literature are based on measurements of the atmospheric conditions [20], others require changing the array configuration [21], and some others are mainly based on algorithms that adjust the effective load of the PV array [22], [23]. Among those methods, the last ones are the most successful for MPOP tracking since they do not rely on measurements of the insolation or the actual load. Such algorithms, commonly known as "perturb and observe (P&O) algorithms," track the evolution of the MPOP through calculations based on measurements of the output-power variations, resulting from discrete shifts produced on the operation point. The main drawback of traditional P&O algorithms is that they cannot cope with rapidly varying atmospheric conditions because of their inability to distinguish output-power variations due to atmospheric conditions changes from on-purpose perturbations. To overcome this problem, a different method, called IncCond, was presented in [24]. This method exploits the property that on the MPOP, the PV panels present the same absolute value of instantaneous and incremental conductance. This property can be obtained from (15)

$$\frac{\Delta i_{\rm pv}}{\Delta {\rm v}_{\rm pv}} + \frac{i_{\rm pv}}{{\rm v}_{\rm pv}} = 0. \tag{18}$$

Particularly, in a previous paper [14], the authors have presented a sliding-mode strategy to control a solar generating system. The sliding surfaces considered in that work were specially designed to fulfill the control objectives presented here. Particularly, in the case of tracking the MPOP, that novel sliding-mode version of the IncCond algorithm allows maximizing the speed of convergence toward the MPOP, which depends on the size of the reactive elements of the converter, the atmospheric conditions, and the load. The intrinsic chattering feature of this control technique can be useful since it provides the required perturbation in the operation point to implement the P&O method. In addition, the proposed sliding-mode controller is attractive since it allows a simple design and contributes with the well-known robustness properties of this control technique.

The control law proposed in that paper can be expressed in the framework of the supervisor control as follows:

$$\begin{cases} \text{if } P_f \geq P_{s\,\rm ref} \Rightarrow Mode\,2: & u_{\rm pv} = \begin{cases} 1, \text{ if } h_1 \geq 0 \\ 0, \text{ if } h_1 < 0 \end{cases} \\ \text{if } P_f < P_{s\,\rm ref} \Rightarrow Mode\,3: & u_{\rm pv} = \begin{cases} 0, \text{ if } h_2 \geq 0 \\ 1, \text{ if } h_2 < 0 \end{cases} \end{cases} \tag{19}$$

where the sliding surfaces

$$h_1 = {\rm v}_b(i_L + I_{b\,\rm ref} - i_w - i_s) = 0 \tag{20}$$

and

$$h_2 = \frac{\Delta i_{\rm pv}}{\Delta {\rm v}_{\rm pv}} + \frac{i_{\rm pv}}{{\rm v}_{\rm pv}} = 0 \tag{21}$$

correspond to power regulation or MPOP tracking, respectively.

D. Comprehensive Operation Strategy

The comprehensive operation strategy for the supervisor control of the hybrid system can be outlined in (22), shown at the bottom of the page.

V. Simulation Results

Computer simulations have been conducted using a comprehensive five-order nonlinear model of the EGHS to assess the performance of the supervisor control. The features of the proposed operation strategy are examined through one example, which combines periods of sufficient and insufficient generation. In Fig. 5, the time evolution of the independent variables can be observed. Fig. 5(a) shows the wind speed (v) varying between 8–13 m/s, with a mean of 10.8 m/s. This sequence was created by adding turbulent components to a slowly varying signal. Fig. 5(b) and (c) depict, respectively, the radiation (λ) and temperature on the PV panels. It can be appreciated that the radiation and temperature profiles are highly correlated. Finally, in Fig. 5(d), the load current referring to the dc bus side (i_L) is shown. The steps in its profile represent abrupt load connection or disconnection.

In Fig. 6, the time behavior of different system variables is displayed. In Fig. 6(a), the total power demand, the total generated power $(\mathrm{wind}+\mathrm{photovoltaic})$, and the battery power delivered to the load during *Mode 3* are depicted. It can be observed in this figure that the generated power tracks the total power demand, except during periods of insufficient generation. It is during those periods that the battery bank postpones its recharge cycle and supplements the generation at the expense of its stored energy. In Fig. 6(b) and (c), the system variables, which are used to decide the operation mode of the generation subsystems, are shown. Fig. 6(b) depicts the variables that resolve the control objective of the wind subsystem (i.e., ω_m and ω_{mSW}). Fig. 6(c) shows the decision variables for of the solar subsystem (i.e., $P_{s\,\mathrm{ref}}$ and P_f). It should be remarked that the supervisor control sets the fictitious power (P_f (in gray)) at a fixed value as long as the solar subsystem is inactive. This practice is followed to avoid incorrect computations of (16) and, consequently, undesirable activations of the solar subsystem. The preset P_f value should be superior than the maximum rated power of the solar subsystem (in this example, 10 kW has been used). The supervisor control determines the operation modes of the EGHS [Fig. 6(d)] by processing the information presented in Figs. 6(b) and 6(c). It is interesting to note that this figure exhibits short periods (see $t \cong 148$ s. and $t \cong 280$ s.) where the supervisor control is switching between *Mode 2* and *Mode 3*. This situation arises because during those periods, the solar subsystem is operating near the MPOP; consequently, P_f and $P_{s\,\mathrm{ref}}$ are very close [Fig. 6(c)]. However, this fluctuation does not produce any adverse effect on the performance of the system, because during

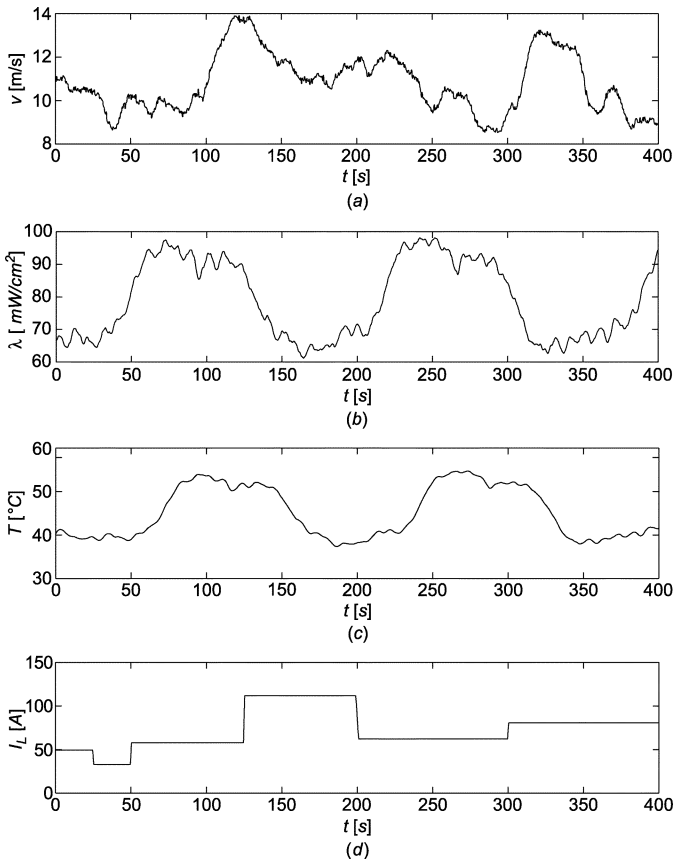

Fig. 5. (a) Wind speed v, (b) insolation λ, (c) temperature T, and (d) load current i_L.

$$
\begin{aligned}
&\text{if } \omega_m \geq \omega_{m\,SW} \Rightarrow Mode\ 1: \begin{cases} \text{Wind Subsystem} \rightarrow \text{Power Regulation} \\ \qquad \left(P_{w\,\mathrm{ref1}} = \mathrm{v}_b(i_L + I_{b\,\mathrm{ref}})\right) \\ \text{Solar Subsystem} \rightarrow \text{Inactive} \\ \text{Battery Bank} \rightarrow \text{Recharge Cycle} \end{cases} \\
&\text{if } \left\{ \begin{matrix} \omega_m < \omega_{m\,SW} \\ P_f \geq P_{s\,\mathrm{ref}} \end{matrix} \right\} \Rightarrow Mode\ 2: \begin{cases} \text{Wind Subsystem} \rightarrow \text{Maximum Power Conversion} \\ \qquad \left(P_{w\,\mathrm{ref2}} = K_{\mathrm{opt}} \cdot \omega_m^3 - \frac{3}{2}\left(i_q^2 + i_d^2\right) r_s\right) \\ \text{Solar Subsystem} \rightarrow \text{Power Regulation} \\ \qquad \left(P_{s\,\mathrm{ref}} = \mathrm{v}_b(i_L + I_{b\,\mathrm{ref}} - i_w)\right) \\ \text{Battery Bank} \rightarrow \text{Recharge Cycle} \end{cases} \\
&\text{if } \left\{ \begin{matrix} \omega_m < \omega_{m\,SW} \\ P_f < P_{\mathrm{sref}} \end{matrix} \right\} \Rightarrow Mode\ 3: \begin{cases} \text{Wind Subsystem} \rightarrow \text{Maximum Power Conversion} \\ \qquad \left(P_{w\,\mathrm{ref2}} = K_{\mathrm{opt}}\, \omega_m^3 - \frac{3}{2}\left(i_q^2 + i_d^2\right) r_s\right) \\ \text{Solar Subsystem} \rightarrow \text{MPOP Tracking} \\ \qquad \left(\frac{\Delta i_{\mathrm{pv}}}{\Delta \mathrm{v}_{\mathrm{pv}}} + \frac{i_{\mathrm{pv}}}{\mathrm{v}_{\mathrm{pv}}} = 0\right) \\ \text{Battery Bank} \rightarrow \text{Able to Supply Power to the Load} \end{cases}
\end{aligned}
\tag{22}
$$

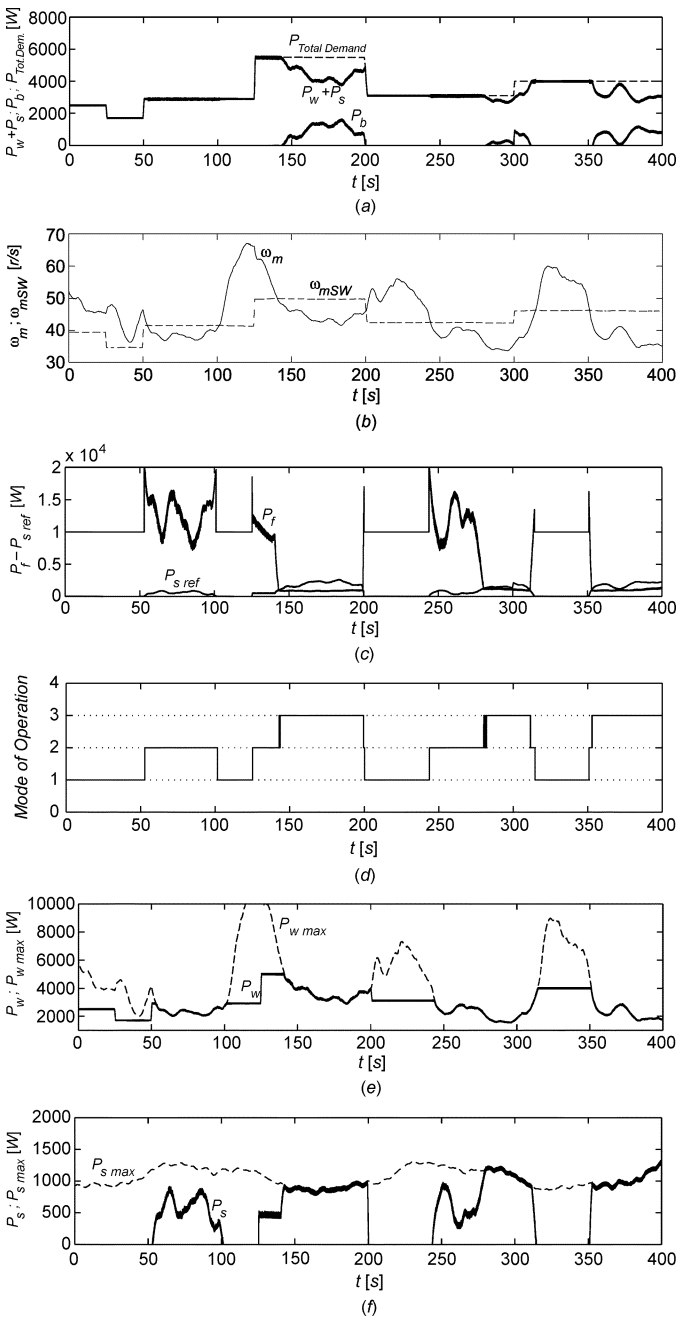

Fig. 6. (a) Generated power $P_w + P_s$, total power demand $P_{\mathrm{Tot.Dem.}}$, and battery power delivery in Mode 3 P_b, (b) shaft speed ω_m versus switching shaft speed ω_{mSW}, (c) PV reference power $P_{s\,\mathrm{ref}}$ versus fictitious power P_f (in gray), (d) operation mode, (e) PV power generation P_s versus maximum PV generation $P_{s\,\mathrm{max}}$, (f) wind power generation P_w versus maximum wind generation $P_{w\,\mathrm{max}}$.

that particular situation, the power reference for the solar subsystem in *Mode 2* and *Mode 3* is on a par.

Finally, the wind and solar-generated power and maximum available power are depicted in Fig. 6(e) and (f), respectively. It can be observed that the wind subsystem tracks the optimum generation reference during modes *2* and *3*, and the solar subsystem does it under *Mode 3*. In addition, in Fig. 6(f), an additional feature incorporated to the supervisor control can be appreciated: a protection to avoid exceeding the rated power of the generation subsystems. Note that at $\mathrm{t} \cong 125$ s, the wind subsystem restrains its generation at 5 kW (the PMSG rated power), despite the wind available power that would allow greater generation. This situation leads the system to operate in *Mode 2*, being the solar subsystem responsible to complement the wind generation to satisfy the total power demand.

VI. Conclusion

The performance of electric generation hybrid systems relies heavily on the existence of a custom-made supervisor control capable to efficiently administrate the diverse energy resources involved. The comprehensive supervisor system developed in this paper proved to be highly competent to manage and coordinate the operation of the subsystems that constitute the EGHS. It provides a versatile decision framework to determine the operation mode of each electrical subsystem. One of its most attractive features is that reliable and unambiguous criteria based only on easily measurable system variables (namely, shaft speed, voltages, and currents) have been proposed for the decision algorithms of the supervisor.

Robust sliding-mode control laws have been considered in this paper to fulfill the different control objectives (i.e., power regulation or maximum energy conversion) of the wind and solar subsystems. However, it is important to remark that the validity of the supervisor decision framework is not merely restricted to those particular control laws. On the contrary, the applicability of the decision framework of the supervisor is general and admits the incorporation of any other control law suitable to attain the aforementioned control objectives.

Finally, for the application considered in this paper, it was decided that the main generation role would be carried out by the wind subsystem while the solar subsystem would play a complementary role. However, this is not at all a rigid limitation of the control proposal, provided that the decision algorithm of the supervisor control can be straightforwardly altered to set the solar subsystem as the main supplier and the wind subsystem as the secondary energy source.

References

[1] R. Ramakumar, J. J. Bzura, J. Eyer, J. Gutierrez-Vera, T. E. Hoff, C. Herig, J. Iannucci, and M. R. Milligan, "Renewable technologies and distribution systems," *IEEE Power Eng. Rev.*, pp. 5–14, Nov. 1999.

[2] J. Jayadev, "Harnessing the wind," *IEEE Spectr.*, vol. 32, no. 11, pp. 78–83, Nov. 1995.

[3] R. Swisher, C. Real de Azua, and J. Clendenin, "Strong winds on the horizon: wind power comes of age," *Proc. IEEE*, vol. 89, no. 12, pp. 1757–1764, Dec. 2001.

[4] R. Spée and J. H. Enslin, "Novel control strategies for variable-speed doubly fed wind power generation systems," *Renew. Energy*, vol. 6, no. 8, pp. 907–915, 1995.

[5] P. Novak, T. Ekelund, Y. Jovik, and B. Schmidtbauer, "Modeling and control of variable-speed wind-turbine drive system dynamics," *IEEE Contr.Syst. Mag.*, vol. 15, no. 4, pp. 28–37, Aug. 1995.

[6] T. Thiringer and J. Linders, "Control by variable rotor speed of fixed-pitch wind turbine operating in speed range," *IEEE Trans. Energy Convers.*, vol. 8, no. 3, pp. 520–526, Sep. 1993.

[7] E. Muljadi, C. P. Butterfield, and P. Migliore, Variable Speed Operation of Generators With Rotor Speed Feedback in Wind Power Applications, National Renewable Energy Laboratory, Golden, CO.

[8] M. Godoy Simoes, B. K. Bose, and R. J. Spiegel, "Fuzzy logic based intelligent control of a variable speed cage machine wind generation system," *IEEE Trans. Power Electron.*, vol. 12, no. 1, pp. 87–95, Jan. 1997.

[9] K. Uhlen, B. A. Foss, and O. B. Gjosaeter, "Robust control and analysis of a wind-diesel hybrid power plant," *IEEE Trans. Energy Convers.*, vol. 9, no. 4, pp. 701–708, Dec. 1994.
[10] F. Valenciaga, P. F. Puleston, R. J. Mantz, and P. E. Battaiotto, "An adaptive feedback linearization strategy for variable speed wind energy conversion systems," *Int. J. Energy Res.*, vol. 24, no. 2, pp. 151–161, 2000.
[11] C. Edwards and S. K. Spurgeon, *Sliding Mode Control: Theory and Applications*. New York: Taylor & Francis, 1998.
[12] V. I. Utkin, J. Guldner, and J. Shi, *Sliding Mode Control Theory in Electromechanical Systems*. New York: Taylor & Francis, 1999.
[13] F. Valenciaga, P. F. Puleston, P. E. Battaiotto, and R. J. Mantz, "Passivity/sliding mode control of a stand-alone hybrid generation system," *Proc. Inst. Elect. Eng., Contr. Theory Appl.*, vol. 147, no. 6, pp. 680–686, 2000.
[14] F. Valenciaga, P. F. Puleston, and P. E. Battaiotto, "Power control of a photovoltaic array in a hybrid electric system using sliding mode techniques," *Proc. Inst. Elect. Eng., Contr. Theory Appl.*, vol. 148, no. 6, pp. 448–455, Nov. 2001.
[15] P. F. Puleston, R. J. Mantz, P. E. Battaiotto, and F. Valenciaga, "Sliding mode control for efficiency optimization of wind energy systems with double-output induction generator," *Int. J. Energy Res.*, vol. 24, no. 1, pp. 77–92, 2000.
[16] H. De Battista, P. F. Puleston, R. J. Mantz, and C. F. Christiansen, "Sliding mode control of wind energy systems with DOIG. Power efficiency and torsional dynamics optimization," *IEEE Trans. Power Syst.*, vol. 15, no. 2, pp. 728–734, May 2000.
[17] H. De Battista, R. J. Mantz, and C. F. Christiansen, "Dynamic sliding mode power control of wind driven induction generators," *IEEE Trans. Energy Convers.*, vol. 15, no. 4, pp. 451–457, Dec. 2000.
[18] B. S. Borowy and Z. M. Salameh, "Methodology for optimally sizing the combination of a battery bank and pv array in a wind/PV hybrid system," *IEEE Trans. Energy Convers.*, vol. 11, no. 2, pp. 367–375, Jun. 1996.
[19] F. Valenciaga, P. F. Puleston, and P. E. Battaiotto, "A VSS control design method based on a differential geometric approach. Application to a wind energy conversion subsystem," *Proc. Inst. Elect. Eng., Contr. Theory Appl.*.
[20] K. Ro and S. Rahman, "Two loop controller for maximizing performance of a grid—connected photovoltaic fuel cell hybrid power plant," *IEEE Trans. Energy Convers.*, vol. 13, no. 3, pp. 276–281, Sep. 1998.
[21] A. Braunstein and Z. Zinger, "On the dynamic optimal coupling of a solar cell array to a load and storage batteries," *IEEE Trans. Power App. Syst.*, vol. PAS-100, no. 3, pp. 1183–1188, 1981.
[22] C. Hua, J. Lin, and C. Shen, "Implementation of a DSP—controlled photovoltaic system with peak power tracking," *IEEE Trans. Ind. Electron.*, vol. 45, no. 1, 1998.
[23] J. H. R. Enslin and D. B. Snyman, "Combined low-cost, high efficient inverter, peak power tracker and regulator for PV applications," *IEEE Trans. Power Electron.*, vol. 6, no. 1, pp. 73–82, Jan. 1991.
[24] K. H. Hussein, I. Muta, T. Hoshino, and M. Osakada, "Maximum photovoltaic power tracking: an algorithm for rapidly changing atmospheric conditions," *Proc. Inst. Elect. Eng., Gen., Transm. Distrib.*, vol. 142, no. 1, 1995.

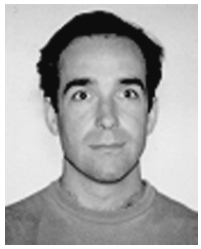

Fernando Valenciaga received the B.B.E.E. and Ph.D. degrees from La Plata National University (UNLP), La Plata, Argentina, in 1993 and 2001, respectively.

Currently, he is Assistant Professor of Automatic Control in the Electrical Engineering Department at UNLP. His research interests are automatic control systems and renewable energy systems.

Paul F. Puleston received the B.S.E.E. degree (Hons.) in 1988 and the Ph.D. degree from La Plata National University (UNLP), Argentina, in 1997.

Currently, he is Professor in the Industrial Design Department, Associate Professor in the Electrical Engineering Department, UNLP, and Research Member of the CONICET. From 1999–2000, he was Research Associate in the Engineering Department, Leicester University, Leicester, U.K.

Dr. Puleston received the Gold Medal "Ing. Antonio Marin" of the National Academy of Engineering. His main interest is automatic control systems.